Folding of a Single-Chain, Information-Rich Polypeptoid Sequence into a Highly Ordered Nanosheet

ARTICLE *in* BIOPOLYMERS · JANUARY 2011

Impact Factor: 2.39 · DOI: 10.1002/bip.21590 · Source: PubMed

9 AUTHORS, INCLUDING:

Ki Tae Nam
Seoul National University
76 PUBLICATIONS **2,309** CITATIONS

SEE PROFILE

Ritchie Chen
Massachusetts Institute of Technology
10 PUBLICATIONS **172** CITATIONS

SEE PROFILE

Ronald N Zuckermann
Lawrence Berkeley National Laboratory
188 PUBLICATIONS **7,303** CITATIONS

SEE PROFILE

Folding of a Single-Chain, Information-Rich Polypeptoid Sequence into a Highly-Ordered Nanosheet.

Romas Kudirka, Helen Tran, Babak Sanii, Ki Tae Nam†, Philip H. Choi, Neeraja Venkateswaran, Ritchie Chen, Stephen Whitelam, and Ronald N. Zuckermann*.

The Molecular Foundry, Lawrence Berkeley National Laboratory, 1 Cyclotron Rd., Berkeley, CA 94720, USA.

**Correspondence to:* rnzuckermann@lbl.gov

†Current address: Dept. of Materials Science & Engineering, Seoul National University, Gwanak 599 Gwanak-ro, Gwanak-gu, Seoul 151-742, Republic of Korea

ABSTRACT

The design and synthesis of protein-like polymers is a fundamental challenge in materials science. A means to achieve this goal is to create synthetic polymers of defined sequence where all relevant folding information is incorporated into a single polymer strand. We present here the aqueous self-assembly of peptoid polymers (N-substituted glycines) into ultra-thin, two-dimensional highly ordered nanosheets, where all folding information is encoded into a single chain. The sequence designs enforce a two-fold amphiphilic sequence periodicity, while varying the patterning of charged residues: alternating charges and contiguous segregated charged domains (block patterning). Sheets form between pH 5 and 10 with the optimal conditions being pH 6 for the alternating sequence and pH 8 for the block. Once assembled, the nanosheets remain stable between pH 6 and 10 with

observed degradation beginning to occur below pH 6. The alternating charge nanosheets remain stable up to concentrations of 20% acetonitrile, while the block pattern displayed greater robustness remaining stable up to 30% acetonitrile. These observations are consistent with expectations based on considerations of the molecules' electrostatic interactions. This study represents an important step in the construction of abiotic materials founded on biological informatic and folding principles.

INTRODUCTION

Mimicking biology's ability to form highly defined, functional three-dimensional architectures, such as proteins, remains an important goal of modern materials science. Fulfillment of this challenge could potentially provide stable, low-cost synthetic materials imbued with the ability to exhibit specific, high-affinity molecular recognition and catalytic activities that rival proteins. Mimicry of biology's architectural control would not only provide new functional materials, but also deepen our insight into protein structure and the rules that govern the kinetics and thermodynamics of their folding.

This paper describes the design and synthesis of two-dimensional, highly-ordered nanosheets from a single-chain synthetic polymer, as a means to examine the degree to which the same assembly and informatic principles of biology can be applied to the folding of synthetic systems. By controlling main chain polymer length, side chain structure and functionality, in conjunction with sequence patterning, we

endeavor to exploit the hierarchical nature of protein folding[1] to generate functional materials. Studied for almost fifty years,[2] computational methods have greatly assisted the understanding of α-polypeptide folding;[3-5] however, the theory to predict the folding and self-assembly of non-natural foldamers is still in its infancy.[6] Therefore, expanding our understanding of biomimetic polymer folding and assembly must currently be done empirically.

In the realm of non-natural foldamers, peptoids' (*N*-substituted polyglycines) ease of synthesis makes them prime candidates for empirical elucidation of polymer folding rules., Using commercially available reagents, the solid-phase submonomer method allows for the efficient synthesis of peptoids with high diversity in side chain functionality.[7] This stands in contrast to the more sophisticated β-peptides, which require multistep protected monomer syntheses.[8] While peptoids may lack some of the inherent structural programming of α- and β-peptides (Figure 1), their synthetic flexibility and efficiency make them an excellent choice to assist in the advancement of biomimetic architectural assembly.

Following nature's blueprint, many investigators are creating high molecular weight synthetic polymers that possess the same monomeric structure, sequence sophistication, and patterned amphiphilicity to access highly ordered biomimetic structures. Most of the activity in this recent area is based on β-peptide or peptoid chemistry. The β-peptide monomer possesses the same structural sophistication and attributes of α-peptides albeit with the inclusion of one additional methylene unit. These parallel attributes culminate in well-defined helical secondary

structures,[9,10] including reports of constrained tertiary interactions using disulfide bonds,[11] metal chelation,[12] and Watson-Crick base pairing.[13] Schepartz and coworkers designed amphiphilic β-peptide sequences that assemble into helical bundles[14] and a crystalographically defined coiled-coil quaternary structure.[15] Furthermore, they linked adjacent helices together in an anti-parallel fashion[16] improving the self-association of the now tetrameric helical bundles 10-fold, thus highlighting the advantages of single chain encoded polymers in the assembly of higher order structures.

Peptoids assume secondary and higher order structures despite their greater conformational freedom, inherent lack of chirality, and absence of backbone hydrogen bond donors as compared to α- and β-peptides. In order to affect main chain curvature, and thus access helical structure, bulky branched chiral substituents have been used as side chains[17-22]. By employing a three-fold amphiphilic sequence periodicity, our lab previously constructed peptoid helices that fold cooperatively into helical bundles[23], which were further stabilized by conjugative chemistry to create a single-chain structure.[24] In an extension of this work, a similar helical bundle motif was used to create a high-affinity zinc-binding site serving as a step toward generating biomimetic nanostructures with enzyme-like functions.[25]

Until recently, β-sheet mimetic architectures have remained elusive as they necessitate the assembly of more challenging chain-chain interactions whereas α-helices only require intra-chain organization. Our lab recently exploited the two-

fold periodicity common in β-sheets[26] to create water-soluble two-dimensional nanosheets only two molecules thick.[27] This highly ordered material was created via the aqueous complexation of two oppositely-charged peptoid strands, which were comprised of only three monomers, *N*-(2-aminoethyl)glycine (Nae), *N*-(2-phenethyl)glycine (Npe), and *N*-(2-carboxyethyl)glycine (Nce). The strands, (Nae-Npe)$_{18}$ and (Nce-Npe)$_{18}$, (Figure 2), assemble into a bilayer, in which the primary driving force for assembly is the burial of the hydrophobic residues and exposure of the ionic, hydrophilic side chains to water. This two-fold periodicity coaxes the polymer into a fully-extended chain conformation to generate a molecular scale linear amphiphile. Since the nanosheet's structure remains intact in the absence of water, it stands to reason that the exposed charged hydrophilic side chains also contribute, via electrostatics, to the overall stability of the supramolecular structure.

The complexation of two separate strands raises the question of whether nanosheet folding information can be encoded into a single polymer chain, as is often the case with protein biopolymers. The use of binary ionic polymer complexation is well studied and has resulted in many new supramolecular materials, such as polyelectrolyte multilayers.[28,29] The advantage of single chains, however, is that it enables more defined biophysical measurements and mechanistic experiments to be performed. More fundamentally, it takes us one step closer to the biological principal, first articulated by Anfinsen[30], that the "instructions" for folding a protein can be encoded by the sequence information within a single polymer chain. Ultimately, we aim to design and synthesize sequences that can not only fold, but also exhibit highly specific molecular recognition and catalysis. In our efforts to

achieve these goals, we present here an important step in generating information-rich single chain polymers that fold into higher order structure via the encoded folding principles of biology.

RESULTS AND DISCUSSION

Design Strategy and Synthesis. In order to obtain high molecular weight, single–strand, information–encoded polymers, we sought to retain and combine the critical design elements from our initial system: hydrophobics, electrostatics, and a two-fold amphiphilic sequence periodicity[27]. We synthesized two constructs containing the same composition and periodicity, but with different charge distributions via the submonomer method: a block charge structure, $(Nae\text{-}Npe)_9\text{-}(Nce\text{-}Npe)_9$, and an alternating charge structure, $(Nae\text{-}Npe\text{-}Nce\text{-}Npe)_9$ (Figure 3). Both of these single-chain polypeptoid constructs are significantly more sophisticated with respect to their monomer sequence information content than classical block and alternating copolymers. The synthesis of these complex sequence patterns with no polydispersity, is a level of precision that remains out of reach of traditional polymer chemistry.

The block charge structure, $(Nae\text{-}Npe)_9\text{-}(Nce\text{-}Npe)_9$, possesses two oppositely-charged stretches of like-charged hydrophilic side chains, providing large recognition domains for strands to interact and pattern themselves laterally according to charge complementarity. These contiguous charged segments may also enforce polymer linearity through intrastrand electrostatic repulsion. In these two

ways this system is similar to our original binary nanosheet system[27]. The alternating charge structure, $(Nae\text{-}Npe\text{-}Nce\text{-}Npe)_9$ retains the ability to mutually associate in a manner that locally satisfies charge-charge interactions, but lacks the large stretches of like-charged domains carried by the block charge molecule. We expect this difference to be significant (see next section). Interestingly, peptidic versions of the alternating charge sequences (e.g. EFKF oligomers) do not form sheets at all and instead form fibrils or hydrogels.[31,32] These two extreme patterns containing the same composition and amphiphilic periodicity should provide insight into the importance of the molecules' local electrostatic charge environment.

Expected Consequences of Charge Patterning. We expect sheets formed from the alternating and block charge constructs to have different electrostatic properties, because of their differing charge patterns. We can explain this expectation using a simple simulation model based on the consideration of the two spatially extended dimensions of a sheet, and only one of the sheet's ionic faces (Figure 4). We set up an extended ordered monolayer of chains of 18 bound charges, modeling peptoids that are 36 residues long. Spacings between charges and chains were taken from experimental measurements as shown (Figure 4a). Charges interact via a screened Coulomb potential[33]. The purpose of this model is to calculate the electrostatic energy associated with specified patterns of peptoids (assuming that such a sheet has already self-assembled). We neglect bending of chains and other spatial fluctuations that might lead to the breakdown of order on large length scales.

We started with a monolayer in which the peptoid termini were aligned row-to-row

(so that green chain ends were aligned in columns), and calculated the inter-molecular electrostatic energy of a peptoid in a given row of the monolayer as we slid that row with respect to the other rows. The direction of translation is shown by the gray arrow in Figure 4a. The monolayer was periodically replicated in both dimensions, in imitation of bulk surroundings, so such a translation affects the pattern of charges displayed by the monolayer but does not disturb the integrity of the monolayer (i.e. there are no 'edges' of the sheet in this calculation). The electrostatic energy U of a peptoid in the translated row was calculated for the alternating charge (blue lines) and the block charge (green lines) constructs, as a function of the distance of row translation x (Figure 4b). Distance $x=0$ describes the initial ordered monolayer, and the maximum value of x shown corresponds to the sliding of a row of the monolayer by one entire peptoid length. We show results at 150 mM NaCl concentration for all residues ionized (solid lines) and for an ionization probability of the COOH residue of 61% (dashed lines). These two choices correspond roughly to pH 7 and 5, respectively (see Materials and Methods).

Interestingly, the model predicts that the favorable electrostatic energy of a block charge sheet (-38 k_BT per peptoid when residues are fully ionized) significantly exceeds that of the alternating charge sheet (-15 k_BT per peptoid). This is chiefly because charges in the interior of each block molecule possess (in rows above and below) only *opposite* charges as their nearest- and next-nearest neighbors (Figure 4d). By contrast, charges in the alternating peptoid monolayer possess *like* charges as their next-nearest neighbors in rows above and below (Figure 4c). We expect that a molecule's *intra*-molecular interaction plays a less prominent role in determining

sheet patterning, because its charges are linked together chemically. At a reduced state of COOH group ionization (dotted lines in Figure 4b), the electrostatic energy of each type of sheet is still favorable, but that of the alternating molecule is only about 5 $k_B T$ per molecule.

The different charge periodicities of the two types of molecule are also reflected in the energetic cost required to translate a row of peptoids within a sheet. For the alternating molecule, sliding rows by twice the backbone charge-charge distance meets with no energetic cost. For the block molecule, any translation less than one molecule length is energetically unfavorable. We therefore expect that the patterns formed within equilibrated sheets of alternating and block molecules will be different. This expectation is illustrated in Figure 4c and 4d, which show sheet fragments from equilibrated Monte Carlo simulations (for full residue ionization) of alternating and block molecules, respectively (see Materials and Methods). The alternating molecule adopts a pattern in which chain ends (green) show no correlation from row to row (Figure 4c), while the rows of the block molecule sheet are strongly correlated (Figure 4d). This high degree of local order suggests that the block molecule is a good candidate for creating sheets that display spatially precise, chemically selective regions.

The model considered here is clearly idealized, and neglects potentially important features of molecular flexibility and hydrophobicity. However, we believe it to be a good starting point for interpretation of our experimental results. It should be noted that the difference per peptoid in entropy of row translation of the two

designs is small relative to the differences in their maximum possible binding energies, so we expect the latter to ensure that the block design is more stable against dissociation than the alternating design.

Structure of Sheets. Sheets were assembled in dilute aqueous solution and analyzed by a variety of techniques: fluorescent optical microscopy, scanning electron microscopy (SEM) and powder pattern X-ray diffraction (XRD). In comparison to the previously reported two-component system, the single-chain peptoid nanosheets form at an approximately three-fold slower rate. Fluorescent optical microscopy of both the alternating charge and block charge nanosheets, using Nile Red, an extrinsic environmentally sensitive dye, showed the presence of sheets with characteristic straight edges (Figure 4). Both the block and alternating charge sheets exhibit typical edge lengths between 10 and 100 microns. Currently, we are unable to control this size distribution; however, investigations are currently under way and will be reported in due course. SEM showed that the sheets retained the same parallel edges as the original two-component system, indicating that we have formed a similar supramolecular morphology from different molecular materials (Figure 5).

The molecular structure of the nanosheets was analyzed by powder pattern X-ray diffraction at the Advanced Light Source. The XRD of both the alternating and block charge nanosheets indicate that the materials possess a high degree of order and a structure similar to that of the two-component nanosheets (Figure 6). Both hybrids possess a 2.7–2.8 nm peak that corresponds to the thickness of the bilayer, and a

4.4–4.6 Å peak that corresponds to the inter-strand distance between polymer chains. The XRD spectra are remarkably similar to that of the previously-reported binary nanosheet system[27], indicating a comparable molecular structure. Examination of the XRD spectra of the materials in the region of the 4.5 Å peak suggests that sheets built from block charge chain and the original two-component nanosheets are more ordered locally than are sheets built from the alternating charge chain. This difference in order may result from a difference in the electrostatic stabilization of the block and alternating charge sheets, consistent with our prediction in the simple simulation model (Figure 4).

pH Dependence on Assembly. The charge state of the molecule should affect the assembly of the nanosheets as electrostatic forces are likely to play a prominent role in sheet stability. If correct charge complementarities were frustrated, this would likely result in lower sheet stability, or may even prevent sheets from forming at all. To explore this notion we examined sheet formation over a pH range of 5–10. We noticed a striking difference in the pH optima and quantity of sheets formed between the alternating and the block charge chains (Figure 7). Nanosheet formation with the alternating charge chain exhibited a strong dependence on pH with maximum sheet production at pH 6, suggesting that the charged state of the polypeptoid has a significant effect on the assembly rate. In contrast, the block charge chain showed less dependence on pH. It formed sheets over the full range of pH's considered, with maximum sheet production at pH 8. This difference in sensitivity to charge state is consistent with our expectations based on considerations of electrostatic energy (Figure 4). We expect the electrostatic

driving force for association of the block charge chains into sheets to be greater than that of the alternating charge chain, and we expect that changes in peptoid charge states impair assembly of the alternating chain before they impair assembly of the block chain.

pH Stability of Sheets. Electrostatic and hydrophobic interactions clearly play significant roles in the stability of sheets. By modulating the pH we affect the charge density of the sheets providing insight into the effects of electrostatic forces. Sheets formed under optimal conditions, pH 6 for the alternating charge chain and pH 8 for the block charge chain, were dialyzed using a 100 kD membrane with the appropriate buffer to a pH between 5–10 until the desired pH was obtained. The sheets were then maintained at the defined pH for 17 hrs, whereupon they were examined using fluorescence optical microscopy (Figure 8). The alternating charge sheets showed no appreciable degradation at pH 6–8, but at pH 5, 9, and 10 sheets were present in decreased quantity and size. In contrast, the block charge chain displayed remarkable resilience to pH, having sheets present at all measured pH values with the only evidence of decomposition (as evidenced by loss of the characteristic straight edges) occurring at pH 5. This weak pH dependence is likely a result of the large contiguous charged domains. In accordance with our electrostatic calculations, we expect spatially extended regions of such domains to remain energetically favorable even when charge states are reduced considerably (Figure 4).

Sheet stability toward acetonitrile. Titration with hydrophobic solvents, such as acetonitrile, serves as a tool for examining the importance of hydrophobic interactions[24]. Therefore, we set out to explore the robustness of the single-chain nanosheets to increasing concentrations of acetonitrile (Figure 9). Sheets were assembled under optimal conditions and then titrated with the appropriate amount of acetonitrile. Both the alternating and block charge sheets showed no apparent degradation at 10% acetonitrile upon examination with fluorescence optical microscopy. Using erosion of straight edges as a measure for perturbation of order, in conjunction with the appearance of sheet fragments, the alternating charge sheets showed greater susceptibility to disruption at concentrations of 20% acetonitrile, with the block charge sheets beginning to show loss of integrity at 30% acetonitrile. There were no discernable structures in either case at concentrations of upwards of 50% acetonitrile. The presence of acetonitrile perturbs the strength of the hydrophobic interactions present within the sheets, thus heightening the importance of electrostatic interactions in sheet integrity and stability. We attribute these differences in stability at 20% acetonitrile to the more favorable electrostatic environment of a block charge nanosheet (Figure 4).

CONCLUSION

We have successfully demonstrated that single-chain, information-rich, high molecular weight non-natural polymers create higher order sheet structures. By exploiting side chain–side chain interactions, we developed a single molecule

system where polymer main chains are fully extended permitting facile interaction with neighboring strands. The two structural motifs, alternating and block charge chains, display differing sensitivities to pH and chemical denaturants with the block charge design possessing the greatest resilience and versatility. This observation is consistent with our expectation based on consideration of inter-peptoid charge-charge interactions. This work demonstrates the impact of sequence information on non-natural polymer folding and self-assembly, and adds an important new folding rule to the peptoid structure toolbox.

MATERIALS AND METHODS

Peptoid Synthesis. Peptoid oligomers were synthesized on an automated robotic synthesizer using the solid-phase submonomer method[7,34]. In this method, the Fmoc group on Rink amide resin (0.61 mmol/g, Novabiochem, San Diego, CA) was deprotected with 20% 4-methylpiperidine in DMF (v/v) before starting the submonomer cycle. Peptoid synthesis on resin was carried out as follows: a 0.6 M solution of bromoacetic acid in DMF (1.13 mL in DMF, 1.35 mmol) and 0.93 eq. of N, N'-diisopropylcarbodiimide (0.20 mL, 1.25 mmol) was added to a resin-bound amine (50 μmol) and mixed for 20 min at 35ºC during acylation step of the submonomer cycle. The resin-bound bromide was then displaced with the amine submonomer by adding a 2 M solution of the amine in N-methylpyrrolidinone. The displacement reaction was carried out for 60 or 120 minutes at 35ºC for residues 1–18 or 19–36, respectively. The crude peptoid products were cleaved from the resin with 95:5 trifluoroacetic acid (TFA):water (v/v) for two hours at room temperature.

The cleavage solution was filtered and evaporated under a stream of nitrogen gas to remove the TFA. The crude peptoid product was then dissolved in a 1:1 mixture (v/v) of water and acetonitrile and subjected to further purification through reverse-phase HPLC on a Vydac C18 column (10 μm, 22 mm × 250 mm), using a gradient of 30–60% acetonitrile in water with 0.1% TFA over 60 min. All final products were analyzed by analytical reverse-phase HPLC (30–55% gradient at 1 mL/min over 30 minutes at 60 °C with a C18, 5 μm, 50×2 mm column) and matrix-assisted laser desorption/ionization mass spectrometry (Applied Biosytem/MDS SCIEX 4800 MALDI TOF/TOF Analyzer) (see Table I). The final peptoid products were lyophilized, dissolved in 100 mM HCl (aq) and then lyophilized again. This step was repeated two more times to ensure formation of the hydrochloride salt. The powder was then dissolved in a 2:1 mixture of DMSO:water in order to obtain a 2 mM stock solution stored at 4 °C.

Table I Characterization of peptoid sequences by HPLC and mass spectrometry.

Peptoid Sequence	Calculated Mass	Observed Mass	Purity[a]
$(Nae\text{-}Npe\text{-}Nce\text{-}Npe)_9$	4981.74	4981.82	91%
$(Nae\text{-}Npe)_9\text{-}(Nce\text{-}Npe)_9$	4981.74	4981.24	95%

[a] after HPLC purification

Sheet Formation. In a 4 mL cylindrical vial, 500 μL of 20 μM peptoid solution in 10 mM buffer and 100 mM NaCl, was prepared from the stock solution. The vials were then slowly rotated about the vertical access on an Appropriate Technical Resources RKVSD Rotamix tube rotator for three days at room temperature. Buffers used

depended on pH: citric acid (pH 5), MES (pH 6), HEPES (pH 7), Tris (pH 8), AMPD (pH 9) and CAPS (pH 10).

Fluorescence Optical Microscopy. Nile Red, an environmentally-sensitive dye whose fluorescence intensity increases substantially when it is localized in hydrophobic environments, was used at a final concentration of 1 μM to stain the sheets for imaging. The solutions were deposited onto pre-cleaned microscope slides and imaged under epifluorescence illumination with an Olympus IX81 inverted microscope fitted with an Andor iXonEM+ EMCCD camera. Loading 8 μL onto the microscope slide, sample solutions were covered with a coverslip and allowed to sit undisturbed for twenty minutes to one hour to allow the sheets to settle.

pH Stability Experiments. Sheets were assembled via the described method and were added to a pre-wetted Spectrum Labs Spectra/Por Float-A-Lyzer G2 dialysis apparatus with cellulose ester membranes and a molecular weight cutoff of 100 kD. The sheets were dialyzed for 3 hrs in the appropriate buffer, at which time the pH of the solutions were equal. The sheet solution was then removed from the dialysis apparatus, transferred to a 2 mL cylindrical vial, maintained for 14 hrs, and then subjected to fluorescence optical microscopy.

Acetonitrile Stability Experiments. Sheets were assembled via the described method and then titrated with acetonitrile to the appropriate percentage. The sheet solution was incubated for 6.5 hrs at room temperature and then subjected to fluorescence optical microscopy.

Powder XRD Analysis. X-ray diffraction data were collected at a multiple-wavelength anomalous diffraction and monochromatic macromolecular crystallography beamline, 8.3.1, at the Advanced Light Source located at Lawrence Berkeley National Laboratory. Beamline 8.3.1 has a 5 tesla single pole superbend source with an energy range of 5-17 keV. Data were collected with a 3 × 3 CCD array (ADSC Q315r) detector at a wavelength of 1.1159 Å. Data sets were collected with the detector 200 mm from the sample. Peptoid sheet solutions were concentrated 100–fold an Amicon Ultra centrifugal filter (100 kD MWCO, Millipore) then centrifuged at 13,200 rpm for 10 minutes. After removing the supernatant, the resulting peptoid sheet pellet was pipetted onto a Mitigen Mesh. Data was processed with custom Matlab (Mathworks) scripts.

Scanning Electron Microscopy. For scanning electron microscopy imaging, peptoid sheet solutions were dropped on plasma-treated Si substrates. The sheets were dialyzed with water beforehand to remove buffer and salt. A Zeiss Gemini Ultra-55 Analytical Scanning Electron Microscope was used with an in-lens detector and beam energies between 1 kV and 3 kV.

Simulations. Simulations were done by assembling a two-dimensional monolayer of 6 x 90 peptoids, periodically replicated in each dimension. Distances between charges and chains were as shown in Figure 4a. Charges interacted via a screened Coulomb potential appropriate for three-dimensional space, $U(x)=(q_1\ q_2\ l_B/r)\ \exp(-x/l_D)$, in units of k_BT at 298 K. Here x is the inter-charge distance; the q_i are charges in units of the elementary charge e; l_B is the Bjerrum length (0.7 nm at 298 K); and l_D is the Debye length (0.79 nm at the 150 mM NaCl considered)[33]. We trunctated this interaction at 5.5 Debye lengths, and verified that our results were unchanged upon increasing the cutoff distance to 6.5 Debye lengths (indicating that we incur no spurious effects from a too-short cutoff). We performed calculations for 1) the case in which all residues were fully ionized, and for 2) the case in which the NH_3 groups were fully ionized but the COOH groups possessed a charge of only -0.61 e. Using the Henderson-Hasselbalch equation to connect residues' pKa values (4.8 for COOH and 10.7 for NH_3) to pH, we believe cases 1 and 2 to approximate pH 7 and 5, respectively. Our treatment (case 2) of the partial ionization of the COOH group is a mean-field one; an alternative is to probabilistically charge residues and average over many simulations with different realizations of this disorder.

Our Monte Carlo simulations (Figure 4c and 4d) consisted of three types of proposed move: 1) swaps of two randomly chosen peptoids; 2) left-right direction reversals of randomly-chosen individual peptoids; and 3) translations in either direction of a randomly-chosen row of the monolayer (we allowed rows to move only by integer multiples of the inter-charge separation, modeling the scenario in

which local order is strongly dictated by molecules' hydrophobic groups). To preserve detailed balance (and hence microscopic reversibility), each move was accepted with certainty if the energy of the system decreased, and with probability $\exp(-\Delta E/k_{\mathrm{B}}T)$ otherwise. Here ΔE is the energy change following the proposed move. In this way we allowed the monolayer fragment treated in our simulation to relax to thermal equilibrium. This procedure is not designed to mimic a realistic dynamics, but is instead designed to determine the configurations that molecules might adopt if they self-assemble close to thermal equilibrium.

Acknowledgments. The authors would like to thank Cheryl Goldbeck and Jeremy Schmit for insightful discussions and Michael Connolly for valuable assistance. This work was carried out at the Molecular Foundry and the Advanced Light Source at Lawrence Berkeley National Laboratory, both of which are supported by the Office of Science, Office of Basic Energy Sciences, of the US Department of Energy under Contract No. DE-AC02—05CH11231. R.K. is supported by the Defense Threat Reduction Agency (IACRO-B0845281).

References

1. Bryson, J. W.; Betz, S. F.; Lu, H. S.; Suich, D. J.; Zhou, H. X. X.; Oneil, K. T.; Degrado, W. F. Science 1995, 270, 935-941.
2. Guzzo, A. V. Biophysical Journal 1965, 5, 809-822.
3. Zhang, Y. Current Opinion in Structural Biology 2008, 18, 342-348.
4. Bonneau, R.; Baker, D. Annual Review of Biophysics and Biomolecular Structure 2001, 30, 173-189.
5. MacKerell, J. A. D. In Annual Reports in Computational Chemistry; David, C. S., Ed.; Elsevier, 2005, p 91-102.
6. Butterfoss, G. L.; Renfrew, P. D.; Kuhlman, B.; Kirshenbaum, K.; Bonneau, R. Journal of the American Chemical Society 2009, 131, 16798-16807.
7. Zuckermann, R. N.; Kerr, J. M.; Kent, S. B. H.; Moos, W. H. Journal of the American Chemical Society 1992, 114, 10646-10647.
8. Hill, D. J.; Mio, M. J.; Prince, R. B.; Hughes, T. S.; Moore, J. S. Chemical Reviews 2001, 101, 3893-4011.
9. Cheng, R. P.; Gellman, S. H.; DeGrado, W. F. Chemical Reviews 2001, 101, 3219-3232.
10. DeGrado, W. F.; Schneider, J. P.; Hamuro, Y. Journal of Peptide Research 1999, 54, 206-217.
11. Cheng, R. P.; DeGrado, W. F. Journal of the American Chemical Society 2002, 124, 11564-11565.
12. Lelais, G.; Seebach, D.; Jaun, B.; Mathad, R. I.; Flogel, O.; Rossi, F.; Campo, M.; Wortmann, A. Helvetica Chimica Acta 2006, 89, 361-403.
13. Bruckner, A. M.; Chakraborty, P.; Gellman, S. H.; Diederichsen, U. Angewandte Chemie-International Edition 2003, 42, 4395-4399.
14. Qiu, J. X.; Petersson, E. J.; Matthews, E. E.; Schepartz, A. Journal of the American Chemical Society 2006, 128, 11338-11339.
15. Daniels, D. S.; Petersson, E. J.; Qiu, J. X.; Schepartz, A. Journal of the American Chemical Society 2007, 129, 1532-+.
16. Petersson, E. J.; Schepartz, A. Journal of the American Chemical Society 2008, 130, 821-823.
17. Armand, P.; Kirshenbaum, K.; Goldsmith, R. A.; Farr-Jones, S.; Barron, A. E.; Truong, K. T. V.; Dill, K. A.; Mierke, D. F.; Cohen, F. E.; Zuckermann, R. N.; Bradley, E. K. Proceedings of the National Academy of Sciences of the United States of America 1998, 95, 4309-4314.
18. Kirshenbaum, K.; Barron, A. E.; Goldsmith, R. A.; Armand, P.; Bradley, E. K.; Truong, K. T. V.; Dill, K. A.; Cohen, F. E.; Zuckermann, R. N. Proceedings of the National Academy of Sciences of the United States of America 1998, 95, 4303-4308.
19. Armand, P.; Kirshenbaum, K.; Falicov, A.; Jr., R. L. D.; Dill, K. A.; Zuckermann, R. N.; Cohen, F. E. Folding and Design 1997, 2, 369-375.
20. Sanborn, T. J.; Wu, C. W.; Zuckermann, R. N.; Barron, A. E. Biopolymers 2002, 63, 12-20.
21. Wu, C. W.; Sanborn, T. J.; Huang, K.; Zuckermann, R. N.; Barron, A. E. Journal of the American Chemical Society 2001, 123, 6778-6784.

22. Wu, C. W.; Sanborn, T. J.; Zuckermann, R. N.; Barron, A. E. Journal of the American Chemical Society 2001, 123, 2958-2963.
23. Burkoth, T. S.; Beausoleil, E.; Kaur, S.; Tang, D. Z.; Cohen, F. E.; Zuckermann, R. N. Chemistry & Biology 2002, 9, 647-654.
24. Lee, B. C.; Zuckermann, R. N.; Dill, K. A. Journal of the American Chemical Society 2005, 127, 10999-11009.
25. Lee, B. C.; Chu, T. K.; Dill, K. A.; Zuckermann, R. N. Journal of the American Chemical Society 2008, 130, 8847-8855.
26. Xiong, H.; Buckwalter, B. L.; Shieh, H. M.; Hecht, M. H. Proceedings of the National Academy of Sciences of the United States of America 1995, 92, 6349-6353.
27. Nam, K. T.; Shelby, S. A.; Choi, P. H.; Marciel, A. B.; Chen, R.; Tan, L.; Chu, T. K.; Mesch, R. A.; Lee, B. C.; Connolly, M. D.; Kisielowski, C.; Zuckermann, R. N. Nature Materials 2010, 9, 454-460.
28. Faul, C. F. J.; Antonietti, M. Advanced Materials 2003, 15, 673-683.
29. Hammond, P. T. Advanced Materials 2004, 16, 1271-1293.
30. Anfinsen, C. B. Science 1973, 181, 223-230.
31. Caplan, M. R.; Moore, P. N.; Zhang, S. G.; Kamm, R. D.; Lauffenburger, D. A. Biomacromolecules 2000, 1, 627-631.
32. Bowerman, C. J.; Ryan, D. M.; Nissan, D. A.; Nilsson, B. L. Molecular Biosystems 2009, 5, 1058-1069.
33. Jackson, J.; Fox, R. American Journal of Physics 1999, 67, 841.
34. Figliozzi, G. M.; Goldsmith, R.; Ng, S.; Banville, S. C.; Zuckermann, R. N. Methods in Enzymology 1996, 267, 437-447.

Figure Legends

Figure 1. Comparison of the monomeric building blocks that comprise polypeptides, β-peptides and peptoids, and the architectural information encoded in their structure.

Figure 2. Oppositely charged pair of polypeptoids that were previously reported[27] to self-assemble into highly ordered nanosheets.

Figure 3. Single-chain peptoids that form nanosheets: (a) alternating charge and (b) block charge sequences. A model of a section of each type of sheet is shown, illustrating the differences in the proposed alignment of the chains. While both designs can accommodate oppositely charged groups to be in close proximity, the alternating charge sheets would be expected to have less long-range order (yellow = carbon, red = oxygen, blue = nitrogen).

Figure 4. Calculations of the electrostatics of model nanosheets show the block charge nanosheet to be more stable than the alternating charge nanosheet. (a) Geometry of model sheet (b) Electrostatic energy *U* of a peptoid in a row of a sheet as that row is slid a distance *x* with respect to the others. (c and d) Monte Carlo simulations that allow peptoids to sample different positions reveal the equilibrium configurations of (c) the alternating charge sheet to be less ordered than (d) the block charge sheet.

Figure 5. Imaging of peptoid nanosheet morphology by scanning electron microscopy (a, d) and fluorescence optical microscopy (b-c, e-f). Sheets were formed from a 20 μM peptoid solution in 10 mM Tris, 100 mM NaCl, pH 8.0. (a-c) Alternating charge sheets made from $(Nae\text{-}Npe\text{-}Nce\text{-}Npe)_9$, (d-f) block charge sheets made from $(Nae\text{-}Npe)_9\text{-}(Nce\text{-}Npe)_9$.

Figure 6. Powder X-ray diffraction analysis of concentrated pellets of the alternating sheets $(Nae\text{-}Npe\text{-}Nce\text{-}Npe)_9$, block sheets $(Nae\text{-}Npe)_9\text{-}(Nce\text{-}Npe)_9$, and two-component sheets $(Nae\text{-}Npe)_{18}$ + $(Nce+Npe)_{18}$, normalized to the amplitude of the 4.4-4.6 Å peak.

Figure 7. Sheet assembly as a function of pH monitored by fluorescence optical microscopy. (a-f) Images of the alternating charge sheets $(Nae\text{-}Npe\text{-}Nce\text{-}Npe)_9$ assembled at (a) pH 5, (b) pH 6, (c) pH 7, (d) pH 8, (e) pH 9, and (f) pH 10. (g-l) Images of the block charge sheets $(Nae\text{-}Npe)_9\text{-}(Nce\text{-}Npe)_9$ assembled at (g) pH 5, (h) pH 6, (i) pH 7, (j), pH 8, (k) pH 9, and (l) pH 10.

Figure 8. Sheet sensitivity to pH as monitored by fluorescence optical microscopy. Images of the alternating charge sheets $(Nae\text{-}Npe\text{-}Nce\text{-}Npe)_9$ at (a) pH 5, (b) pH 7, (c) pH 8, (d) pH 9, and (e) pH 10. Images of the block charge sheets $(Nae\text{-}Npe)_9\text{-}(Nce\text{-}Npe)_9$ at (f) pH 5, (g) pH 6, (h) pH 7, (i) pH 9, and (j) pH 10.

Figure 9. Sheet stability to acetonitrile as monitored by fluorescence optical microscopy. Images of the alternating charge sheets $(Nae\text{-}Npe\text{-}Nce\text{-}Npe)_9$ at (a) 10%, (b) 20%, (c) 30%, and (d) 40% acetonitrile. Images of the block charge sheets $(Nae\text{-}Npe)_9\text{-}(Nce\text{-}Npe)_9$ at (e) 10%, (f) 20%, (g) 30%, and (h) 40% acetonitrile.

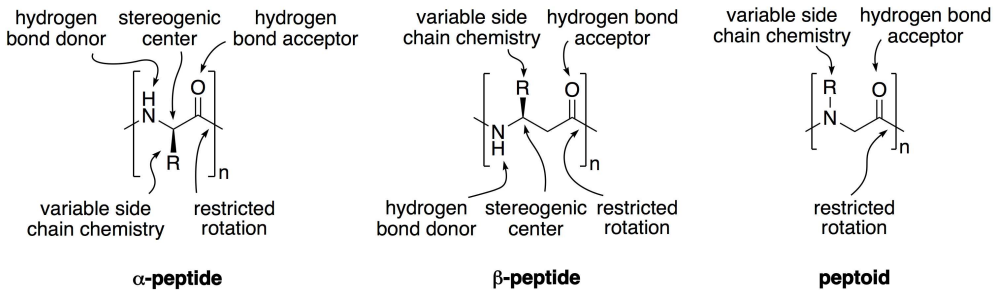

Figure 1. Comparison of the monomeric building blocks that comprise polypeptides, ß-peptides and peptoids, and the architectural information encoded in their structure.
1073x322mm (72 x 72 DPI)

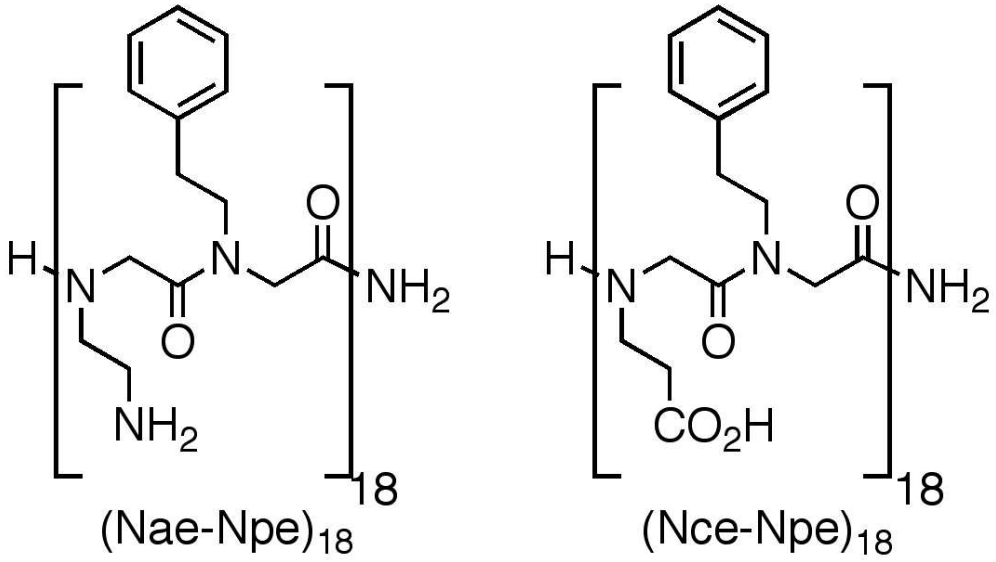

Figure 2. Oppositely charged pair of polypeptoids that were previously reported[27] to self-assemble into highly ordered nanosheets.
91x51mm (300 x 300 DPI)

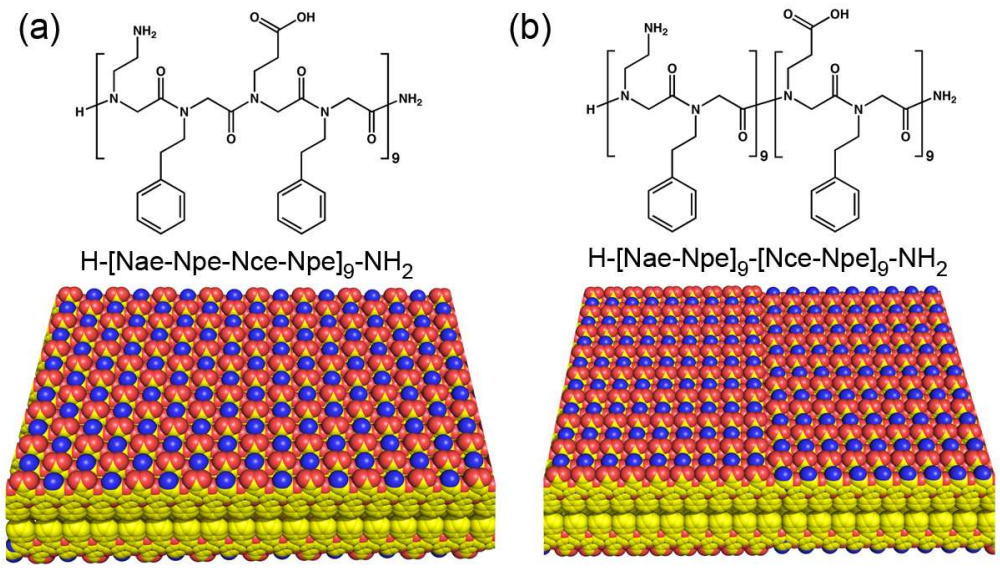

Figure 3. Single-chain peptoids that form nanosheets: (a) alternating charge and (b) block charge sequences. A model of a section of each type of sheet is shown, illustrating the differences in the proposed alignment of the chains. While both designs can accommodate oppositely charged groups to be in close proximity, the alternating charge sheets would be expected to have less long-range order (yellow = carbon, red = oxygen, blue = nitrogen).
101x57mm (300 x 300 DPI)

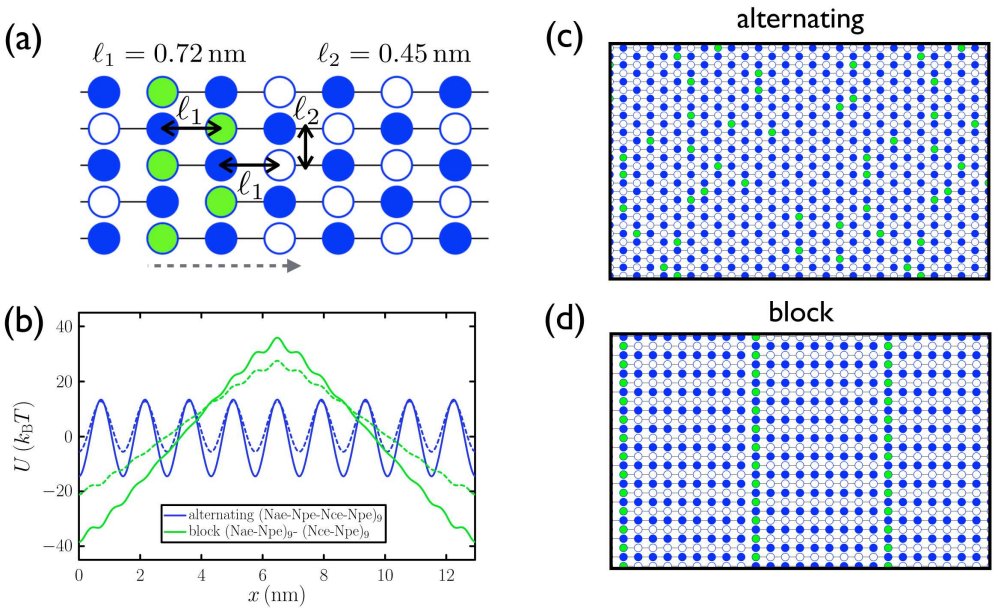

Figure 4. Calculations of the electrostatics of model nanosheets show the block charge nanosheet to be more stable than the alternating charge nanosheet. (a) Geometry of model sheet (b) Electrostatic energy *U* of a peptoid in a row of a sheet as that row is slid a distance *x* with respect to the others. (c and d) Monte Carlo simulations that allow peptoids to sample different positions reveal the equilibrium configurations of (c) the alternating charge sheet to be less ordered than (d) the block charge sheet.
198x120mm (300 x 300 DPI)

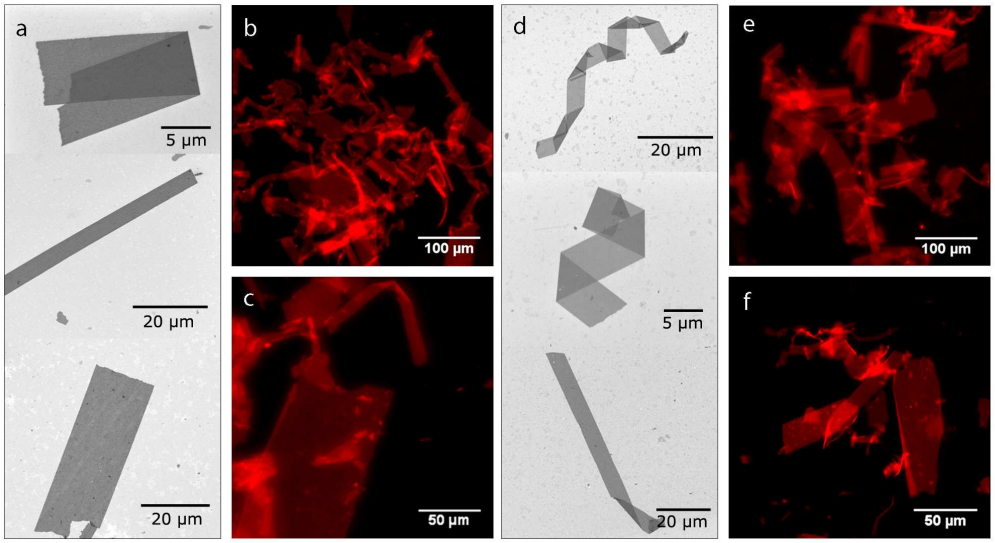

Figure 5. Imaging of peptoid nanosheet morphology by scanning electron microscopy (a, d) and fluorescence optical microscopy (b-c, e-f). Sheets were formed from a 20mM peptoid solution in 10 mM Tris, 100 mM NaCl, pH 8.0. (a-c) Alternating charge sheets made from $(Nae\text{-}Npe\text{-}Nce\text{-}Npe)_9$, (d-f) block charge sheets made from $(Nae\text{-}Npe)_9\text{-}(Nce\text{-}Npe)_9$.
168x92mm (300 x 300 DPI)

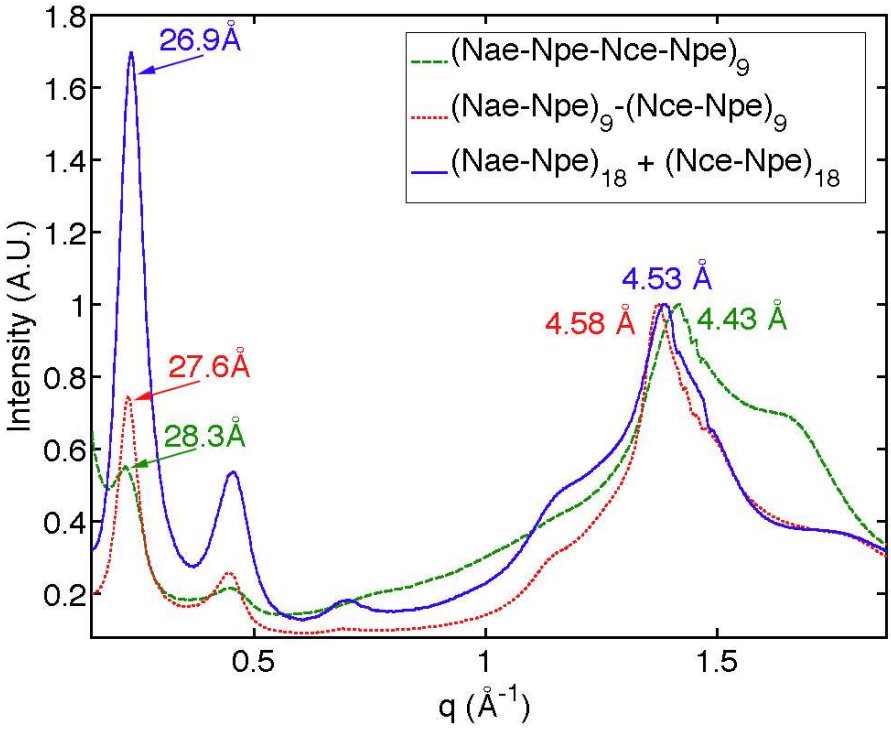

Figure 6. Powder X-ray diffraction analysis of concentrated pellets of the alternating sheets (Nae-Npe-Nce-Npe)$_9$, block sheets (Nae-Npe)$_9$-(Nce-Npe)$_9$, and two-component sheets (Nae-Npe)$_{18}$ + (Nce+Npe)$_{18}$, normalized to the amplitude of the 4.4-4.6 Å peak.
83x64mm (332 x 332 DPI)

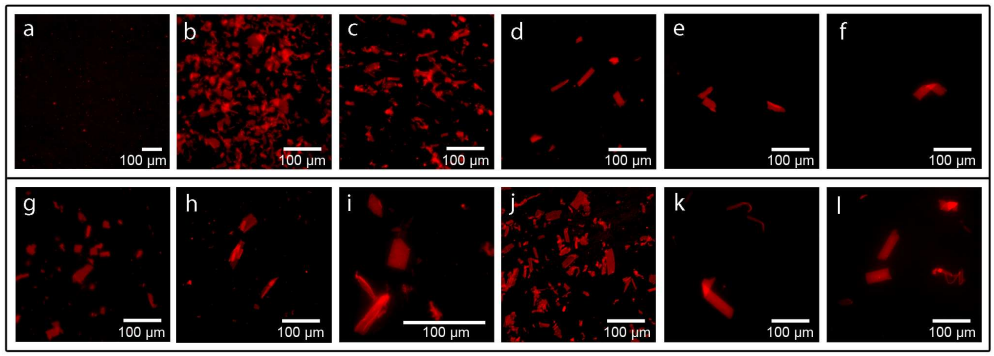

Figure 7. Sheet assembly as a function of pH monitored by fluorescence optical microscopy. (a-f) Images of the alternating charge sheets (Nae-Npe-Nce-Npe)$_9$ assembled at (a) pH 5, (b) pH 6, (c) pH 7, (d) pH 8, (e) pH 9, and (f) pH 10. (g-l) Images of the block charge sheets (Nae-Npe)$_9$-(Nce-Npe)$_9$ assembled at (g) pH 5, (h) pH 6, (i) pH 7, (j), pH 8, (k) pH 9, and (l) pH 10.
173x62mm (300 x 300 DPI)

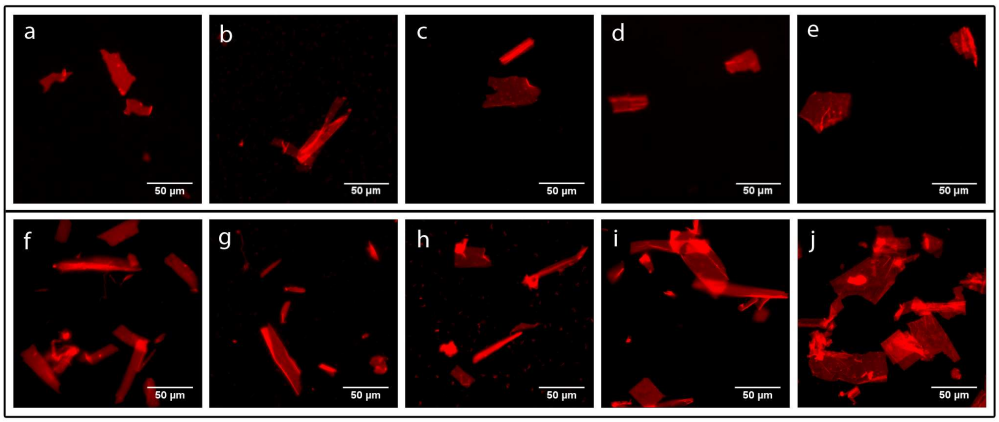

Figure 8. Sheet sensitivity to pH as monitored by fluorescence optical microscopy. Images of the alternating charge sheets $(Nae\text{-}Npe\text{-}Nce\text{-}Npe)_9$ at (a) pH 5, (b) pH 7, (c) pH 8, (d) pH 9, and (e) pH 10. Images of the block charge sheets $(Nae\text{-}Npe)_9\text{-}(Nce\text{-}Npe)_9$ at (f) pH 5, (g) pH 6, (h) pH 7, (i) pH 9, and (j) pH 10.
172x72mm (300 x 300 DPI)

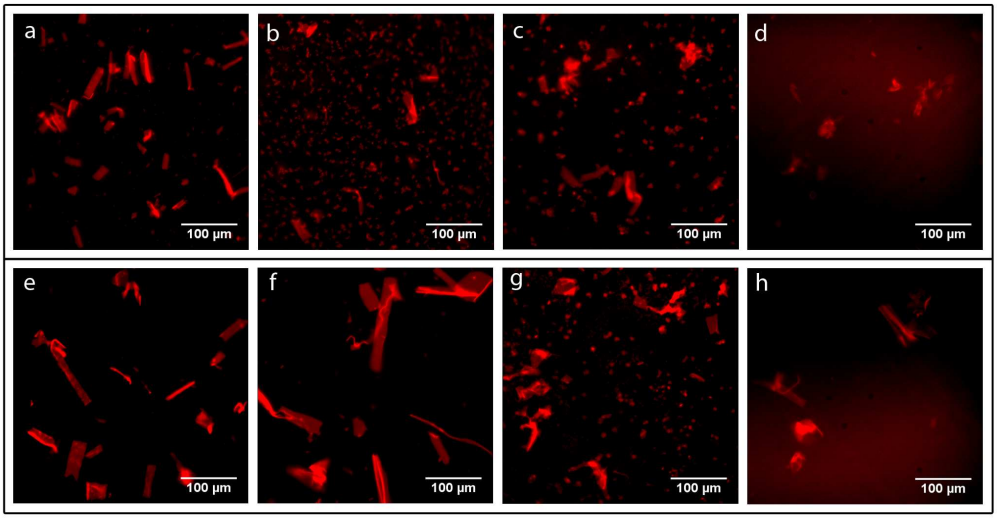

Figure 9. Sheet stability to acetonitrile as monitored by fluorescence optical microscopy. Images of the alternating charge sheets $(Nae\text{-}Npe\text{-}Nce\text{-}Npe)_9$ at (a) 10%, (b) 20%, (c) 30%, and (d) 40% acetonitrile. Images of the block charge sheets $(Nae\text{-}Npe)_9\text{-}(Nce\text{-}Npe)_9$ at (e) 10%, (f) 20%, (g) 30%, and (h) 40% acetonitrile.
172x90mm (300 x 300 DPI)